Towards enhancing hot tooling to form high-γ' superalloys

Arthi Vaasudevan[1*], Fernando D. León – Cázares[4], Enjuscha Fischer[3], Thomas Witulski[3], Catherine Rae[1*] and Enrique Galindo – Nava[1,2*]

1* Department of Materials Science and Metallurgy, University of Cambridge, 27 Charles Babbage Rd, CB3 0FS, United Kingdom.
2 Department of Mechanical Engineering, University College London, 510a Roberts Engineering Building Torrington Place, London, WC1E 7JE, United Kingdom.
3 Materials Science, Otto Fuchs KG, Derschlager Str. 26, Meinerzhagen, 58540, Germany.
4 Sandia National Laboratories, 7011 East Avenue, Livermore, CA, 94550, USA.

*Corresponding authors. E-mails: av511@cam.ac.uk; cr18@cam.ac.uk; e.galindo-nava@ucl.ac.uk.
Contributing authors. E-mails: thomas.witulski@otto-fuchs.com; enjuscha.fischer@otto-fuchs.com; fleonca@sandia.gov.

Abstract

Ni-superalloys are well-established for use in high temperature applications in aerospace, power generation and automotive sectors, yet, are seldom considered as materials for hot tooling. The operational conditions of hot forming dies potentially exceed those experienced by aircraft turbine discs. Fortunately, new disc alloys have pronounced elevated temperature capabilities and the current study focuses on implementing two advanced alloys, VDM 780 and Haynes 282 (H282) as hot tool materials. There is, however, inadequate evidence of their life-limiting properties and mechanisms in the in-service temperature regime of 700 – 900 ℃. Thus, realistic operating conditions were replicated by combining interrupted short and long-term thermal-mechanical tests. Initially, isothermal ageing in the furnace was used to compare the extent of γ' coarsening between the alloys, and subsequent in-situ ageing and compression testing measured the accompanying loss in strength. Compression creep testing at stresses near the yield points (250 – 750 MPa) revealed accelerated creep rates at high temperatures. The results indicated that even as exposure duration, temperature, and applied stress all influence microstructural evolution, the exposure temperature was pivotal in determining the effective life of these γ' strengthened alloys. Dissolution kinetics of γ' around near-solvus temperatures was crucial and was governed by elemental additions. As a result, the research paves the way for a better understanding and design of superalloys with improved thermal integrity for hot tooling.

Keywords: VDM 780, H282, Superalloys, Hot tooling, Gamma prime, Thermal stability, Creep testing, Microstructure, Delta, Carbides, Turbine discs, Hot forging.

1. Introduction

There is an increasing emphasis on developing high temperature materials to cater to the transportation and power requirements [1]. The largest users of high temperature materials are the gas turbine engines in modern jet aircrafts and the land-based turbine power generators. Other areas of application include turbocharger rotors, pressure vessels, heat exchanger tubing, etc. Nickel superalloys satisfy the requirements with their ability to withstand appreciable loading at operating temperatures close to the melting point ($T_o / T_m > 0.6$) for extended periods of time and resist mechanical and chemical degradation, without undergoing failure. The implementation of these materials results in improved fuel economy and reduced carbon emissions [1, 2].

The superior performance of Ni superalloys, especially the ones employed as aircraft engine components, stem from having a high γ' volume fraction (V_f), and demand the forming of these parts at temperatures around 1000 – 1100 ℃ [3]. This consequentially, exerts severe expectations on the hot tooling, imposing tool temperatures in the range of 700 – 900 ℃. Popular steel dies are inadequate to handle such increased thermal-mechanical stresses. The current work takes a novel approach to exploring the application of low γ' superalloys as hot forming materials.

Over the last 50 years, alloy Inconel 718 (IN718) has been a widely used material among low γ' alloys owing to its combination of significant strength, workability, corrosion resistance, affordability, and excellent weldability [4]. Despite these appealing attributes, IN718 suffers from the thermal instability of γ'' phase. At 650 °C, the metastable phase

overages and rapidly transforms into the thermodynamically stable, but plate-like and brittle δ. Hence, the alloy's application for prolonged time is restricted to temperature lower than 650 °C to retain strength and creep resistance properties. ATI Specialty Materials developed alloy 718 Plus with a 50 ºC advantage over IN718 (up to 704 ºC) [5], via promoting the more stable $L1_2$ phase γ'. More recently, the development of the new alloy VDM 780, with the prospect of retaining good properties until 750 ºC has gained attention for its use at even higher temperatures [6].

VDM 780, developed by VDM Metals, is an improved derivative of IN718 for higher service temperatures. The γ' solvus is ~995 °C and solvus of δ is ~1020 °C [7]. Like 718 Plus, there has been an ambiguity concerning the nature of the high temperature phase, either δ and/or η [8, 9]. The high temperature phase was proved by C. Ghica, et al [10] using HRTEM to be a layered structure consisting of alternating η and δ phases, with a majority of η in the precipitates [10]. For the sake of unambiguous discussion in this work, the high temperature phase will be referred to as δ. Nevertheless, no trace of γ'' has been observed. The presence of a bimodal distribution of γ' was revealed, with the Vickers hardness values increasing in heat treated specimens holding increased V_f of smaller precipitate sizes [9]. Apart from the potential of having high strength capabilities up to 750 ºC, there is no data published in open literature about the elevated temperature strength, thermal stability, and creep resistance of VDM 780.

The current study concentrates on investigating the thermal stability and creep properties of VDM 780 at temperatures between 700 – 900 ºC, and importantly draws a comparison between VDM 780 and an established, low γ' alloy, Haynes 282 (H282), with a view to potentially implementing them as materials for hot forming tools. H282 is an appealing γ'-strengthened alternative to IN718, with adequate manufacturability. Its modest elevated temperature strength is compensated by excellent microstructure stability over long exposure times [11]. The alloy is said to demonstrate resistance to γ' coarsening and to forming deleterious TCP phases even with 1000 hours of exposure at temperatures between 760 – 870 ºC [11], and hence, was chosen for comparison with VDM 780. In the current study, VDM 780 and H282 were subject to isothermal ageing, in-situ strength testing, and compression creep testing, in the temperature range of 700 – 900 ºC, followed by thorough microstructural examination to understand the effects of stress, temperature and ageing time on the microstructural evolution and stability.

2. Experimental methods and procedures

Alloys VDM 780 and H282 were made available by Otto Fuchs KG in the form of forging stocks. The nominal compositions of the alloys are presented in Table 1. The alloys were forged to produce billets and were subsequently heat treated as follows: **VDM 780:** Solution treatment (ST) 1020 ºC/ 1H/ AC, Precipitation anneal (PA) 720 ºC/ 8H/ FC → 620 ºC/ 8H/ AC; & **H282:** ST 1050 ºC/ 1H/ AC, PA 1010 ºC/ 2H/ AC + 788 ºC/ 8H/ AC.

Table 1: Nominal compositions of VDM 780 and H282 in weight percent.

Wt %	Cr	Co	Al	Ti	Nb	Mo	C	B
VDM	18	25	2.1	0.2	5.4	3	-----	-----
H282	20	10	1.5	2.1	-----	8.5	0.06	0.005

2.1. Metallographic preparation and microstructural examination

Samples in as-received (AR), as-aged, and crept conditions were cut in the direction transverse to the longitudinal axis of the cylinders using Struers-Secutom precision cutting machine. The cut pieces were mounted in conductive Bakelite and were ground progressively with fine SiC papers starting from 1200 to 4000 grits, then polished with 1μm diamond solution followed by a final 0.06 μm colloidal silica polish. Samples were subsequently electrochemically etched using the γ etchant, 10 % orthophosphoric acid in distilled water. The microstructures were examined under the secondary electron and backscatter electron modes available on a scanning electron microscope (SEM) Zeiss Gemini 300.

2.2. Isothermal ageing

Cylinders were sealed in quartz tubes filled with Ar gas and subsequently were isothermally aged in an induction furnace. Following aging, the samples were rapidly quenched in ice water to freeze and retain the as-aged microstructures.

2.3. Mechanical testing

All compression tests in this work were carried out using TA instrument's DIL 805 A/D, a differential dilatometer amenable to quenching (A) and deformation (D) modes as it ensured good temperature and strain control. Miniaturized specimens were machined out of the heat-treated billets to yield solid cylinders of diameter 5 mm and

length 10 mm, appropriate for dilatometry. Prior to testing, the cylindrical specimens were thoroughly rinsed in acetone and then in ethanol in an ultrasonic bath. They were ground with 1200-grit emery sheet to remove the peripheral oxide layer to expose the bare alloy surface to spot welding, given a final rinse in industrial methyl sulphate and blow dried. Accurate measurements of initial length and diameter of all prepared dilatometer samples were recorded with a vernier caliper having an accuracy of 0.02 mm to be input into the program. Maximum care was taken to maintain parallelism between the ends of the cylinders and not to grind away excess material. Spot welding of S-type 0.2 thermocouple at the center of the cylinder was carried out under Ar atmosphere and two Mo-alloy discs (of diameter 10 mm and thickness 0.5 mm, each) were spot welded onto the ends of the cylinders to provide lubrication and prevent easy cooling of samples from the tools. The ensemble of Mo-discs, sample and thermocouples were carefully placed inside the dilatometer, ensuring that the platens were strictly parallel.

Hot compression tests were conducted using strain-control at test temperatures from 700 – 900 ºC to derive proof stresses and flow curves behaviour. Final true strain for deformation was set to 0.15 for all conditions. Held under vacuum, the cylinders were ramped to test temperatures at 30 ºC/s, homogenised for 10 minutes (to attain thermal equilibrium), and deformed until the set strain was achieved or the applied force exceeded 20 kN (maximum permissible force). Time, displacement, force, true strain, and true stress were recorded at 3000 deformation steps. A strain rate of 0.01/s (or deformation rate 0.1 mm/s) was selected as it closely replicated the industrial deformation rate. The samples were then cooled to room temperature at the rate of 10 ºC/s under pure argon gas and were stabilised for a minute before venting the chamber.

Compression creep testing was conducted under load-control at temperatures from 700 – 900 ºC, and at constant stresses between 250 – 750 MPa, input as equivalent force in Newtons. Test specimens were again held under vacuum, ramped to test temperatures at 30 ºC/s, soaked for 10 minutes and deformed for 3 or 7 hours, depending on the test. Time, true strain, applied stress, change in length measured with silica pushrods and change in diameter measured using a monochromatic laser beam were recorded for 6000 deformation steps. Following the deformation, the samples were cooled to room temperature at the rate of 10 ºC/s under pure argon gas and were stabilised for a minute before venting the dilatometer chamber.

All test data collected were processed and analysed using OriginPro [12], a proprietary computer software for scientific graphing and data analysis.

2.4. Image Analysis

SEM micrographs were processed using the image analysis software ImageJ to estimate γ' area % and mean size. A normal distribution of the particle size was generated with automatic binning, along with the summary of mean particle size and standard deviation. The data was imported to OriginPro, wherein the measurements of areas of observed precipitates were assumed to be perfectly circular and were processed to yield their resultant diameter.

3.   Results

3.1. Initial microstructure

VDM 780 and H282 are both low γ' alloys, i.e., <35 % V_f, yet they are fundamentally different in terms of their composition; standard heat treatments; grain size; the presence, morphologies, and distributions of secondary phases. Starting microstructures of VDM 780 and H282 were examined to understand these differences. Micrographs imaged at lower and higher magnifications are shown in Fig 1. (VDM 780) and 2. (H282).

VDM 780 was composed of nearly equiaxed γ grains with a weighted average grain diameter of 93.8 ± 2.1 µm and a fair number of annealing twins. The grain sizes were measured from EBSD data using Aztec crystal software. High angle grain boundaries were designated as boundaries having misorientation above 15º; twin boundaries were excluded from the grain size calculation. The grain boundaries in VDM 780 were δ-free but were populated by coarse γ'. This was expected as the solution heat treatment temperature was around the δ solvus. This attribute can potentially cause grain coarsening at elevated temperatures due to the absence of an effective grain boundary pinning phase. When viewed at higher magnification, the grain interiors showed a bimodal distribution of γ', containing secondary precipitates (γ'_{sec}) of mean diameter 35 ± 5.24 nm, formed on cooling from solution treatment and tertiaries (γ'_{ter}) of diameters ranging between 10 – 15 nm, nucleated during cooling from solution treatment and developed further during aging treatment. The average area % of γ'_{sec} was measured to be 26.8 %. The γ' particle size distribution in VDM 780 is shown in Fig 3.a.

H282 revealed a combination of fine and coarse grains with grain diameters ranging between 30 – 273 µm. The mean grain diameter was greater than that of VDM 780 and was measured to be 171.2 ± 13.9 µm. The sub-grain microstructure at a finer scale contained monomodal γ'_{sec} distribution with an average particle diameter of 37 ± 4.6 nm. The average area % was calculated to be 22.2 %. The γ' particle size distribution in H282 is shown in Fig 3.b. The grain boundaries were decorated with discontinuous films of $M_{23}C_6$ and grain interiors showed a mix of other carbides such as MC, M_6C, along with borides, nitrides, carbo-nitrides, or carbo-borides. To understand the nature of carbides and other secondary phases present apart from γ', and their morphology and distribution in the AR material; energy dispersive X-ray spectroscopy (EDX) was performed, and the results are presented in Fig 4.

From the images, a Cr rich discontinuous carbide network was observed in the grain boundaries, and Mo rich globular carbides were observed intragranularly and were taken to be $M_{23}C_6$ and M_6C, respectively, similar to observations made in [13] and [14]. Apart from these, Ti-rich nitrides were also located inside the grains and owing to high density of Ti, they appeared dark under the SEM. It was reported by Hanning, Fabian, et al [15], that Mo-rich borides were absent in H282 following TEM analysis. But EDX images presented in Fig. 4 suggest a possibility of Mo-rich boride precipitation surrounding TiN precipitates. It is indeed ambiguous whether Mo borides envelope Ti Carbo-nitrides or Mo carbo-borides envelope Ti rich nitrides. A thorough TEM examination is necessary to draw conclusions on the identity of these secondary phases.

Nevertheless, the preliminary differences in the starting microstructures of VDM 780 and H282 were understood.
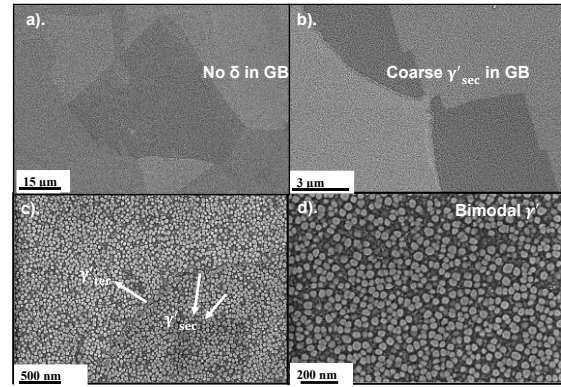

Fig 1. Initial microstructure of VDM 780 in the as-heat treated state a). secondary electron (SE) image showing grain boundaries devoid of δ phase, b). In-lens SE (IL) image at higher magnification showing coarse γ'_{sec} at grain boundaries, c). IL image showing γ'_{sec} and γ'_{ter} at the boundaries, and d) IL image displaying bimodal distribution of intragranular precipitates in γ matrix.
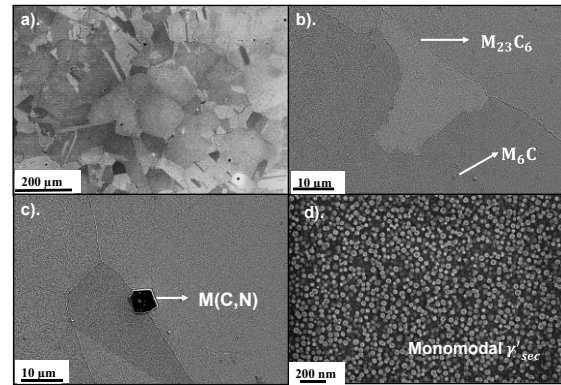

Fig 2. Initial microstructure of H282 in the as-heat treated state a) SE image displaying a mix of small and coarse grains, b) SE image depicting the presence of $M_{23}C_6$ on boundaries and M_6C intragranularly, c) SE image indicating the presence of a carbo-nitride, and d) IL image of monomodal distribution of γ' in γ matrix.
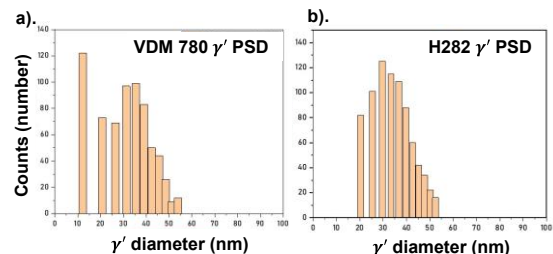

Fig 3. γ' particle size distribution in the alloys, a) shows bimodal distribution exhibited by VDM 780, and b) shows monomodal distribution exhibited by H282.
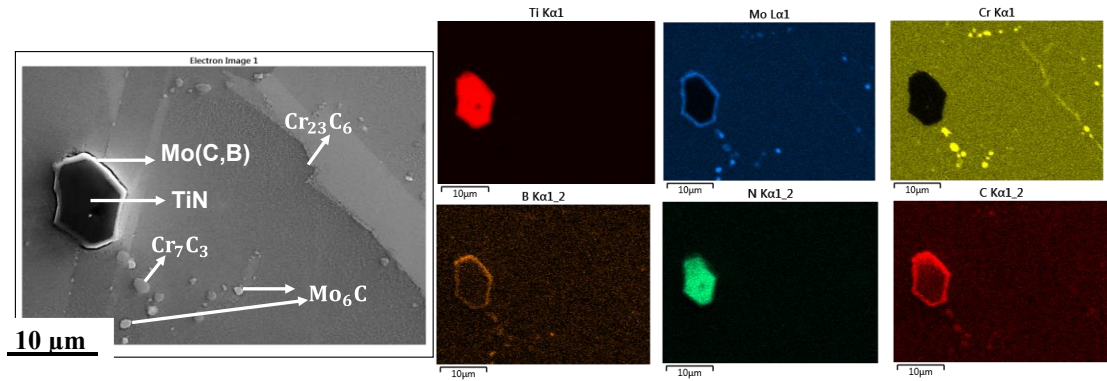
Fig 4.EDX mapping of different types of carbides present in H282.

3.2. Elevated temperature strength

There is lack of information on yield strengths and flow stress behaviours of these alloys, especially VDM 780, at temperatures between 700 – 900 °C. Hot forming dies, and other tools are mostly under the influence of compressive stresses, and H282 and VDM 780 were subjected to uniaxial compression testing. The knowledge of flow curves and strengths at this temperature range is very useful to identify the possibility of plastic deformation during forming cycles when compared against the simulation predicted results of Von Mises stresses on the tools, wherever applicable.

The flow curves are presented in Fig 5. a. (VDM 780), and b (H282), along with proof stress information in Fig 6. At 700, 800 and 850 °C strain hardening was observed in both alloys while at 900 °C strain softening and dynamic recovery occurred. Proof stresses (as measured to be true stresses corresponding to 0.2 % true strain) are higher for VDM 780 at lower temperatures but are nearly equal at 900 °C. High strength of VDM 780 could be attributed to high γ' V_f and finer precipitate size than that in H282.
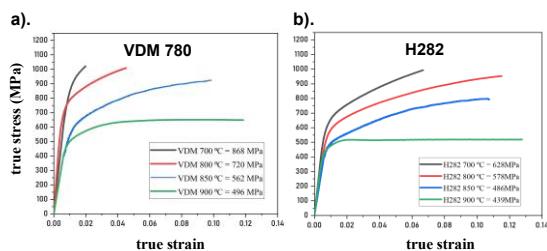

Fig 5. Flow curves displaying the variation of true stress vs true strain a) in VDM 780 and b) in H282.
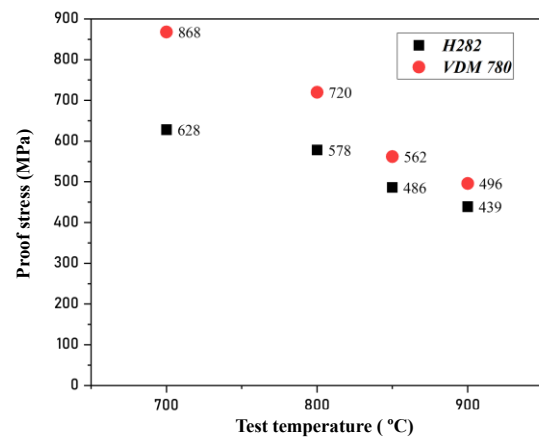

Fig 6. A plot of variation of proof stresses as a function of test temperatures for VDM 780 (red) and H282 (black).

3.3. Effect of thermal exposure on microstructure and mechanical properties

Hot forming tools and dies are expected to remain in service for a long time with good structural integrity for which the thermal stability of microstructure is essential. In γ' strengthened alloys, the microstructural instability is reflected as a loss of phase %, undesirable phase transformation or in-situ precipitation of deleterious phases and leads to a loss of strength and ductility [11].

During hot forming, workpieces are generally maintained between 1000 – 1200 °C [16, 17] and the temperature of hot work tool steels are raised to ~550 °C due to severe thermal gradients between the workpiece and the tool; this is detrimental to the tool life [3]. To prevent this, in the current study with superalloys, the background temperature of the tool is to be increased further. Based on simulation, the expectation is that the temperature of the tools will vary between 700 – 900 °C. The surface temperature

might raise closer to ~900 °C. Thus, temperature regime of 700 – 900 °C is considered. Specimens of both alloys were isothermally aged for 40 hours at 700 °C, 18 hours at 800 °C, to mimic long-term in-service conditions, and at 900 °C for 3 hours to mimic the short-term spikes in tool surface temperatures during operation.

To gain a deeper understanding of time-driven microstructural changes, a shorter exposure duration of 7 hours was also chosen at both 700 and 800 °C to be compared to the 40 hours and 18 hours microstructures, respectively.

Microstructures of both alloys were examined after isothermal aging in the furnace. The aged microstructures of VDM 780 are presented in Fig 7 and that of H282 are presented in Fig 8. Average secondary γ' particle diameters along with the standard deviations, and area % for each aged condition were measured using ImageJ.

a. **VDM 780**

In VDM 780, at 700 °C after 7 hours exposure little change in precipitate size or V_f was observed in comparison with the AR microstructure, while after 40 hours of exposure, even though the γ'_{ter} was intact, a modest increase in the size of both secondaries and tertiaries was observed. At 800 °C distinct changes in the microstructure were noticed. Soaking for 7 hours led to the disappearance of γ'_{ter} and the sizes of γ'_{sec} were higher than the AR specimen, but comparable to those present in 700 °C, 40 hours sample. Increasing the soaking period to 18 hours at 800 °C drove a substantially increased coarsening rate of the secondary precipitates. Additionally, δ phase was observed after 7 hours and 18 hours.

Fig 9 explains the relevant features noted after 800 °C treatment. Incoherent δ precipitates were sporadically observed to be precipitated from the grain boundaries and propagated intragranularly into the grains, serving no purpose apart from consuming the γ' forming elements, Al and Nb and thus, leading to the decline in the γ' V_f. At 900 °C even a small exposure period of 3 hours caused a severe decline in secondary V_f along with much larger precipitate sizes.

a. H282

In H282, there was no visible change in γ' size and V_f between the AR specimen and those aged for 7 hours at 700 °C and 800 °C. However, the sample aged at 700 °C for 40 hours and 800 °C for 18 hours displayed a slight increase in size compared to the

initial microstructure and to samples aged at shorter times at the respective temperatures. At 900 °C with 3 hours of exposure, there was a substantial decline in the secondary γ' V_f with pronounced coarsening.

Fig 10. displays the evolution of grain boundary $Cr_{23}C_6$ carbides with temperature. The density of the carbides decreased from an almost continuous network along grain boundaries at 700 °C, 40 hours to discontinuous precipitation at 800 °C, 18 hours to a much-depleted discrete precipitates at 900 °C, 3 hours.
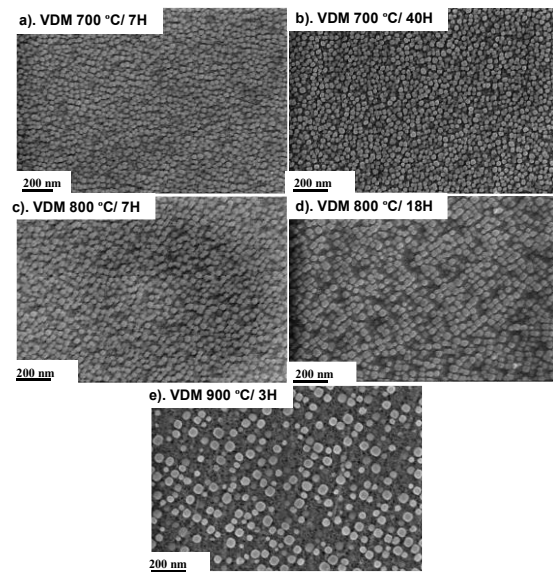

Fig 7. IL images displaying as-aged microstructures of VDM 780 after furnace ageing for conditions a). 700 °C/ 7H; b).700 °C/ 40H; c).800 °C/ 7H; d).800 °C/ 18H; and e).900 °C/ 3H.
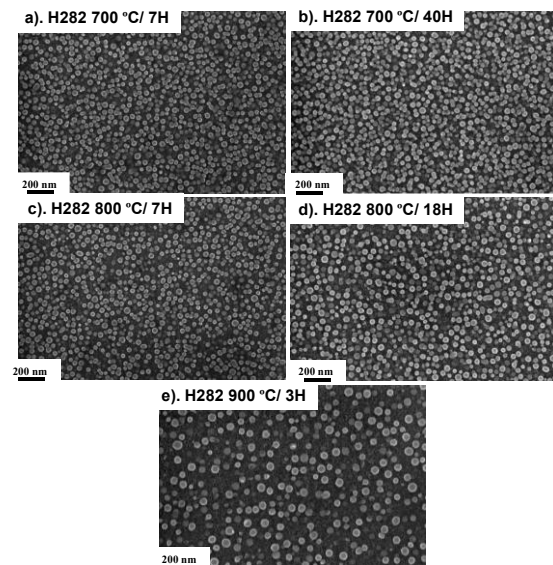

Fig 8. IL images displaying as-aged microstructures of H282 after furnace ageing for conditions a). 700 °C/ 7H; b). 700 °C/ 40H; c). 800 °C/ 7H; d). 800 °C/ 18H; and e). 900 °C/ 3H.

3.3.1. Effect of exposure time and temperature on γ'

Fig 11 and Fig 12 present details on the effect of ageing temperature and times on γ' coarsening for VDM 780 and H282, respectively. It is evident that VDM 780 is unaffected by exposure at 700 ºC. The particle size and area % are unchanged between AR and 40 hours at 700 ºC; and there is an overlap between sizes of 7 hours and 40 hours at 700 ºC, along with no additional phase precipitation or transformation, implying that the microstructure is very stable with temperature and time at 700 ºC. A substantial increase in size and decline in area % from AR is witnessed at 800 ºC/18H; so is the increase in particle sizes from 800 ºC/7H to 800 ºC/18H. The temperature is favourable for δ nucleation and growth, and it can be postulated that this accelerates the coarsening and dissolution of γ'. At 900 ºC, a serious 8 % decline in area % occurs along with a 25 nm increase in the size.
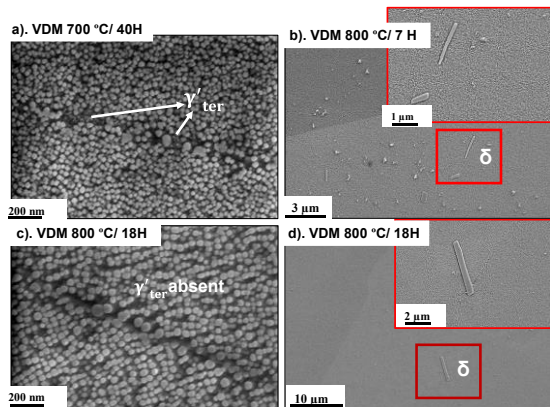

Fig 9. Explains the differences observed in the microstructures of VDM 780 after iso-ageing, a). 700 ºC/40H: IL image showing γ'_{sec} and γ'_{ter}, and no δ; b). 800 ºC/7H: showing the presence of δ; c). 800 ºC/18H: revealing the absence of γ'_{ter} precipitates; and d). 800 ºC/18H: showing the presence of δ phase.

In H282, the microstructure is stable with respect to ageing time and temperature at 700 and 800 ºC. Despite increased size between AR and 700 ºC/40H, there is no change in area % or size among 700 ºC/7H, 700 ºC/40H, 800 ºC/7H, and 800 ºC/18H. This again validates the hypothesis that H282 exhibits γ' stability at elevated temperatures. However, at 900 ºC, like VDM 780, H282 also succumbs to γ' coarsening and dissolution as the temperature is near the phase solvus. It is noteworthy that even as the γ' content and sizes at 900 ºC are comparable between the alloys, the rate of the decrease is more pronounced in VDM 780 than in H282.
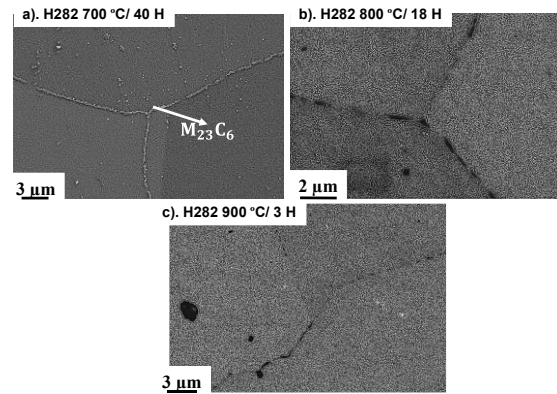

Fig 10. IL images revealing the decreasing $Cr_{23}C_6$ density with ageing temperature in H282 for ageing conditions a). 700 ºC/40H; b). 800 ºC/18H; and c). 900 ºC/3H.
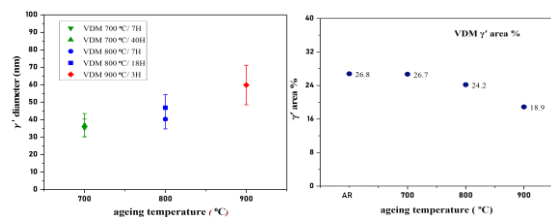

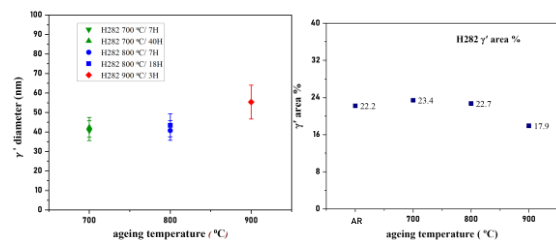Fig 11. Examining the effect of ageing temperature and time on the γ' size and V_f in VDM 780.

Fig 12. Explaining the effect of ageing temperature and time on the γ' size and V_f in H282.

3.3.2. Impact of precipitate evolution on yield strength

To learn the effects of thermal ageing on mechanical strength, in-situ ageing and uniaxial testing were done at soaking temperatures and proof stresses were determined. In-situ ageing and uniaxial tensile testing was done by Otto Fuchs KG on both VDM 780 and H282. In-situ ageing and compression testing on VDM 780 was carried out in the dilatometer for conditions 700 ºC/40H, 800 ºC/18H, and 900 ºC/3H. Where duplicated, the tests were closely repeatable giving confidence in the accuracy of the technique and the results. During in-situ ageing, holding times were matched with corresponding ageing times in the furnace, to mimic furnace ageing and avoid any changes in the microstructure arising from quenching and re-heating.

Fig 13. shows the flow stress curves of VDM 780 before and after ageing at the test temperatures. Figure 13.a. shows the difference of proof stresses between aged and unaged samples as a function of test temperatures. The slight increase in strength after 40 hours ageing at 700 ºC can be attributed to the growth in size of tertiaries that may fall under the category leading to transition from weak to strongly coupled pairs of dislocations. The decrease in strength observed at 800 ºC after 18 hours can be attributed to the dissolution of tertiaries, coarsening of secondaries and the onset of δ precipitation. However, additional tensile tests presented in Fig 14. a. (VDM 780) and b. (H282), exhibit near-equal strengths for VDM 780 at 850 ºC and above. As expected, near-equal proof stresses in H282 were observed from the tensile tests for different test temperatures and times. Therefore, we can conclude that the relative variation in strength for the conditions tested is only small.
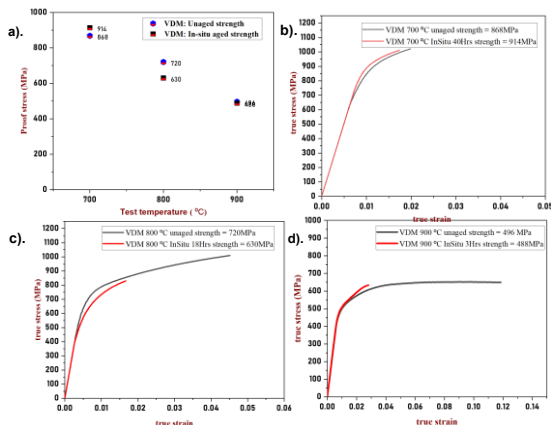

Fig 13. a) Variation of compressive proof stresses of VDM 780 with test temperature prior to and after ageing. b) Flow curves of VDM 780 tested at 700 ºC in unaged and 40 H aged condition. c) Flow curves of VDM 780 tested at 800 ºC in unaged and 18 H aged condition. d) Flow curves of VDM 780 tested at 900 ºC in unaged and 3 H aged condition.
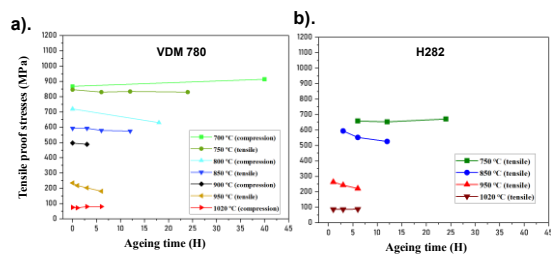

Fig 14. Presenting the variation of tensile proof stresses with exposure times in hours for different temperatures in a) VDM 780 and b) H282.

3.4. Creep testing and microstructural evolution

The macroscopic creep deformation response of VDM 780 and H282 are presented as true strain vs time curves in Fig 15. Tables 2. a. (H282) and b. (VDM 780) display the creep strain values along with strength information for different test conditions. The influence of both temperature and stress on creep could be deduced as specimens were crept at a combination of high and low stresses at temperatures between 700 – 900 ºC. Creep was interrupted at low strains and exposure times were curtailed to subject alloys to limited deformation. For each of the conditions tested, observed minimum creep rates were computed and are plotted as a function of creep temperature as shown in Fig 15.c. As expected, the creep rates increased with increasing temperatures. Overall, for similar testing conditions, VDM 780 displayed negligible creep strains at lower temperatures compared to H282. In contrast, at the highest test temperature the creep strain of VDM 780 is almost twice than that experienced by H282.
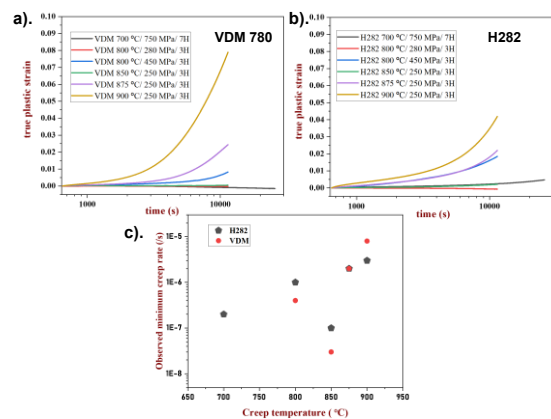
Fig 15. Plots displaying creep plastic strain verses time for a) VDM 780 and b) H282; c) presenting the variation of observed minimum creep rate as function of creep temperature for VDM 780 (red) and H282 (black).

Table 2.a. H282 Creep strain

T (ºC)	Stress (MPa)	t (Hrs)	Strain H282	Strength H282
700	750	7	0.5 %	628
800	280	3	Nil	578
800	450	3	1.8 %	578
850	250	3	0.2 %	486
875	250	3	2.2 %	-
900	250	3	4.2 %	439

Table 2.b. VDM Creep strain

T (ºC)	Stress (MPa)	t (Hrs)	Strain VDM	Strength VDM
700	750	7	Nil	868
800	280	3	Nil	720
800	450	3	0.8 %	720
850	250	3	0.05 %	562
875	250	3	2.4 %	-
900	250	3	7.8 %	496

3.4.1. Creep response of H282

At 700 ℃, with relative stress level, $\sigma_{applied}/\sigma_{yield}$ (σ_a/σ_y) of 119.4 %, the alloy sustained principally primary creep with limited secondary creep. At 800 ℃, for creep condition of σ_a/σ_y around 50 %, no creep was observed. The applied stress was further increased to 450 MPa at 800 ℃ to result in σ_a/σ_y of 77.85 %. This led to a noticeable 1.8 % creep strain. Hence, it can be noted that at lower temperatures, applied stress dictated creep strain. However, at higher temperatures of 875 and 900 ℃, the resulting creep strain was significant. At 50 % relative stresses, there was a two-fold increase in strains experienced between 875 and 900 ℃.

Microstructures of the samples were examined at selected conditions 700 ℃/750MPa/7H, 800 ℃/450MPa/3H, and 900 ℃/250MPa/3H; to reveal the effects of temperature and stresses. From the micrographs (in Fig 16), no new stress-induced microstructural changes were witnessed apart from expected coarsening of γ'_{sec} with concomitant decline in γ'_{sec} and $M_{23}C_6$ V_f, quite consistent with the microstructures observed after isothermal ageing.
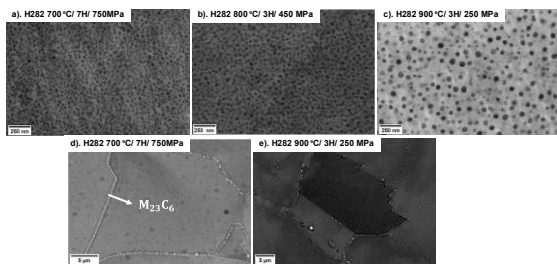

Fig 16. Backscatter SEM (BSE) micrographs of un-etched H282 specimens after creep at (a) 700 ℃/7H/750 MPa, (b) 800 ℃/3H/450 MPa, and (c) 900 ℃/3H/250 MPa; all displaying γ'_{sec}. BSE micrographs of H282 (d and e) displaying continuous and discrete precipitation of $Cr_{23}C_6$ in the boundaries in 700 ℃/7H/750 MPa and 900 ℃/3H/250 MPa conditions, respectively.

3.4.2. Creep response of VDM 780

Creep behaviour of VDM 780 was distinct from that observed in H282. Between 700 – 850 ℃, low creep strains were experienced with none of the tests fully reaching steady state creep, notwithstanding, a few tests showing nil creep strains. 700 ℃ testing with σ_a/σ_y of 86.4 %, 800 ℃/280 MPa/3 H with σ_a/σ_y of 38.9 % and 850 ℃/250 MPa/3 H with σ_a/σ_y of 44.5 % all displayed no plastic strain. An increase in the applied stress to 450 MPa (σ_a/σ_y of 62.5 %) at 800 ℃/3H resulted only in 0.8% creep strain, which indicated that VDM 780 was less sensitive to creep stress at lower test temperatures. At temperatures above 850 ℃, there was a non-linear increase in the creep plastic strains observed. At 875 ℃ with σ_a/σ_y of approximately around 50 %, a substantial plastic strain was observed equal to that of H282 at the same condition, with more secondary creep regime. At 900 ℃, maximum creep plastic strain of 8 % was experienced. This implies that VDM 780 is more temperature sensitive and employing it above 850 ℃ could be precarious over long duration.

Any observations of negative creep were considered non-physical and were attributed to perturbations arising from Mo-discs undergoing deformation or any inaccuracies while recording the initial dimensions of the samples as the DIL 805 is very sensitive. For compression deformation with the DIL 805 A/D, the change in length is continuously decreasing and is reflected as positive creep strain. A negative creep strain means that the sample expanded against the applied compressive load. Such instances of negative creep are well documented for tensile creep in single crystal superalloys undergoing directional coarsening of γ', with precipitate rafts aligning perpendicular to the stress axis [18], which is not a possibility in these alloys. Nonetheless, microstructure examination under TEM would be necessary to conclusively negate the presence of any creep strain.

Fig 17 displays the SEM micrographs of the crept VDM 780 samples, sequentially in various test conditions. It was observed that at 700 ℃, the microstructure was comparable to the AR one with retained tertiaries, secondaries, and coarsened secondaries at the grain boundaries. At 800 ℃ testing with lower stress, the microstructure was intact, but at higher stresses a peculiar stress-induced effect of grain boundary migration followed by discontinuous grain boundary γ' precipitation was observed. The discontinuous precipitation was seen in all samples tested at 850 ℃ and above. Discontinuous precipitation constitutes "the

formation of a two-phase lamellar structure behind moving grain-boundaries" and is well explained in Williams, David B. et al. [19]. The precipitation reaction is of interest as it leads to a detriment in mechanical properties.

At 900 ºC, presented in Fig 18, thick rods of δ precipitation growing inside the grains were observed along with discontinuous γ' precipitation. Also, at 900 ºC, there were γ'-free deformation bands. Fig 19 presents the rough schematic for the δ phase TTT curve for alloy VDM 780. With phase solvus at 1020 ºC, the nose of δ precipitation (shown as green curve in the figure) could be somewhere between 850 – 900 ºC for time between 1 – 3 hours. At 800 ºC, δ starts to form between 3 – 7 hours.
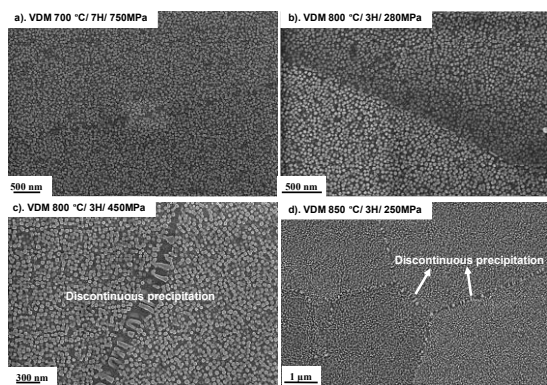

Fig 17. IL micrographs of VDM 780 crept specimens, a). 700 ºC/ 7H/ 750 MPa showing both γ'_{sec} and γ'_{ter}; b). 800 ºC/3H/ 280 MPa displaying γ'_{sec}; c). 800 ºC/ 3H/ 450 MPa; and d). 850 ºC/ 250 MPa revealing discontinuous grain boundary precipitation with intragranular γ'_{sec}.
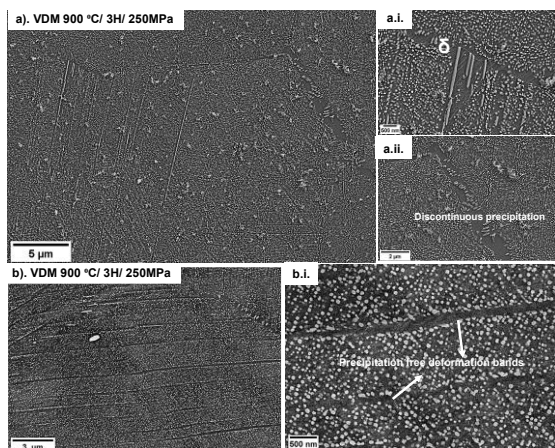

Fig 18. VDM 780 creep at 900 ºC/ 3H/ 250 MPa: IL micrographs showing a.i). thick rod-like δ and a.ii). discontinuous precipitation of lamellar γ' behind migrated grain boundaries; b.i). BSE micrographs showing γ'-free deformation bands.
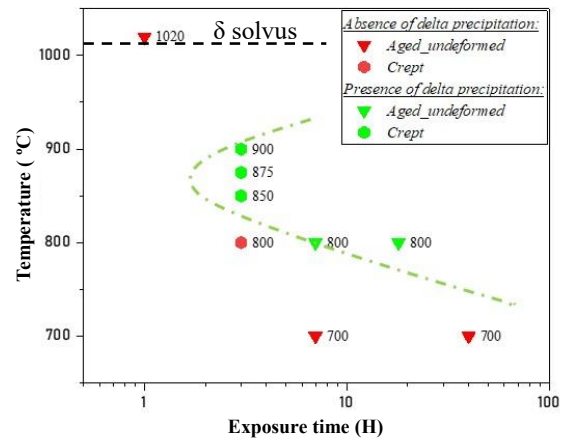

Fig 19. Time temperature transformation curve of δ phase in VDM 780, showing the presence or absence of δ for different exposure temperatures and times.

4. Discussion

A comparison is drawn between the alloys VDM 780 and H282 for hot tooling applications. However, the larger aim of this paper is also to identify and design optimised nickel superalloys for this application. Usually in hot forming, the workpiece is maintained at a higher temperature than the tools and due to this thermal gradient, there is a superficial increase in the temperature of the tools. In the current study with superalloy candidates, the aim is to increase the background or core temperature capability of the tools. The tools are expected to experience temperatures between 700 – 800 ºC at most locations, for major parts of their life, with the surface that encounters the workpiece, to experience temperatures above 800 ºC up to 900 ºC. From the experimental evidence, it was observed that both VDM 780 and H282 performed satisfactorily for this requirement and were better than the conventional nickel superalloy, IN718. But between the alloys, VDM 780 was better at lower temperatures while H282 was more reliable at higher temperatures.

The elevated temperature strength of VDM 780 is about 200 MPa greater than H282 at lower temperature and the difference diminishes as temperature increases. With no practical variation in grain size due to temperature, the grain boundary strengthening can be calculated using Hall-Petch relationship using $\sigma_D = \frac{K_Y}{\sqrt{D}}$, where D is the mean grain size and K_Y is the Hall-Petch constant. The value used for K_Y in calculations for yield strength models proposed by Galindo-Nava et al [20] is 710 MPa $\mu m^{1/2}$. Using the value for K_Y, the relationship yields a difference of about 20 MPa between the alloys due to differences in grain size. This implies that the effect of grain size towards strengthening is minor. Similarly, the effect of solid solution

strengtheners is also likely to be small. In these alloys, the primary strength arises from γ'; size, distribution and V_f, all dictate the penetrability of dislocations. In the case of fine sized precipitates with low fraction, the leading and trailing dislocations do not occupy γ' simultaneously and constitute weak pair coupling, while in case of large precipitate sizes, they give rise to strongly coupled dislocation pairs wherein both dislocations reside in a particle at the same time. Critical resolved shear stresses (CRSS) quantify the stresses required to drive these dislocations into the precipitates and generally, a maximum is observed when there is a transition between weak to strong coupling. The bimodal distribution of γ' is advantageous in VDM 780 at lower temperatures for providing high strength. At 700 ℃, with increasing ageing time, the size of tertiaries increases. This will increase the strength when the growth in size of γ'_{ter} is sufficient to result in strong coupling. However, at higher temperatures of 800 and 900 ℃, due to dissolution of γ'_{ter} and coarsening of γ'_{sec}, the particle shearing stress will be absent and the strength of the alloy will diminish.

From the iso-aged microstructures of H282, it can be observed that, apart from a decreased density of $M_{23}C_6$ carbides, no noticeable difference in γ' area percent or particle diameter occurs between 700 and 800 ℃ ageing treatments. For all practical purposes, equal measurements could be assumed across 700 ℃/ 7H, 700 ℃/40 H, 800 ℃/ 7H, and 800 ℃/18 H treatments. With ageing time, the retention in strength and resistance of γ' coarsening in H282 is induced by high Ti/Al ratio and high Mo additions. The higher the Ti/Al ratio, the lower is the γ-γ' misfit and the rate of coarsening of γ' is reduced. The slow diffusivity of Mo retards the coarsening of γ'. Additionally, Ti also increases the antiphase boundary energy (APBE) and confers resistance to precipitate shearing. This plays a positive role in time dependent creep deformation. Thus, high Ti/Al ratio and high Mo additions in H282 impart thermal stability [21, 22].

In VDM 780, the high Al and Nb content (2 Wt % and 5.4 Wt % as opposed to 0.2 % and 0 % in H282, respectively) confers higher γ' V_f and higher elevated temperature yield strength [6]. However, higher Al/Ti ratio makes the γ' susceptible to coarsening due to increased γ-γ' misfit. The lack of Ti in VDM 780 is compensated by Nb additions. Nb segregates to γ' and its low mobility helps retain finer precipitates [22]. Thus, in VDM 780, at low temperatures, γ' kinetics is controlled by Nb. But as the temperature increases closer to γ' solvus and δ

forming temperatures, Nb is depleted by the formation of δ (Ni_3Nb, DO_a orthorhombic phase). Also the presence of 25 % Co stabilises δ phase in VDM 780 once it is formed [23]. Hence, above 850 ℃, there are no elemental contributions precluding γ' coarsening and dissolution, thus VDM 780 is more susceptible to loss of strength and creep resistance when compared to H282.

In creep, no new or unexpected microstructural changes arise in H282 in addition to the trend observed after iso-ageing. The microstructure is stable with no undesirable incoherent phases or TCP phases, similar to reports by Pike, L et al [11]. However, in VDM 780, as temperature increases, lamellar γ' and δ phases appear. When δ precipitates form, they are enveloped by a γ'-depleted zone, which is inherently weaker. Likewise, the occurrence of coarser lamellar γ' will contribute little towards strengthening. Additionally, at 900 ℃, γ'-free deformation bands are observed to exist in majority of grains. Sundararaman et al. [24], has reported that these bands originate due to shearing of precipitates on <111> planes, possibly accompanied by cross slipping to <100> planes, all taking place within the formed band. Once cut, the halves get redistributed and dissolved, thus leaving an empty band. The applied stress alone cannot be solely attributed to the phenomenon. It is agreed that the fragmentation occurs owing to the mechanical influence, however, the dissolution of the redistributed fragments, each of which is below the critical radius, is temperature driven. This occurrence could be one of the reasons for the detrimental response of this alloy to the applied stress at 900 ℃. Thus, VDM 780 is less able to withstand the high surface temperatures of the tools.

Some of the damage encountered by the tool surfaces include adhesive and abrasive wear, erosion, plastic deformation, thermal-mechanical fatigue, and surface or gross cracking [25]. In this study, the susceptibility to plastic deformation in candidate alloys is studied through the means of short-term strength testing and long-term creep testing. Also, the extent of deterioration of properties with time is examined using isothermal ageing. It can be concluded that VDM 780 is more prone to die chilling effect and can be used for operations having lower demanding surface temperatures, while H282 can be employed for more demanding surface temperature applications.

In future, to implement γ' superalloys as tool materials, the following factors must be considered: 1. γ' coherency with γ matrix and APBE required by dislocations to disorder γ' precipitates, 2. γ' V_f and

variation with increasing temperature, and 3. γ' size, stability, and extent of coarsening. These parameters rely largely on the alloy chemistry but can be modified by applying the appropriate processing conditions.

5. Conclusions

A study is presented wherein two low γ' strengthened derivatives of IN718, a newly developed alloy VDM 780 and another commercially popular alloy H282, are compared for the purpose of application as hot tooling materials. These alloys have gained popularity for their appreciable fabricability and weldability, however, they remain largely unexplored with respect to their mechanical properties in the temperature regime of 700 – 900 °C, the range of interest to hot tooling. The tools are expected to withstand continuous loading cycles at high temperatures for prolonged times. Therefore, elevated temperature strength, thermal stability through furnace ageing, and time-dependent creep deformation are evaluated. The mechanisms driving deformation are studied by examining the evolution of γ' and other secondary phases with applied temperature, time, and stress. An insightful correlation between process parameters, mechanical outcomes and microstructure is established.

Between 700 – 800 ℃, VDM 780 is observed to be much stronger and creep resistant, potentially due to the presence of bimodal distribution of fine tertiaries and higher V_f of secondaries. The γ' (monomodal) V_f is smaller in H282, comparatively. Nevertheless, both the alloys display microstructural stability with no new undesirable precipitation that might weaken the microstructure.

Above 800 °C and below 900 °C, wherein the tests mimic short-term spikes in tool temperatures during operation, H282 is observed to possess better creep resistance with reasonable strength due to a more stable microstructure. In VDM 780, the microstructure is weakened by a). occurrences of stress-induced discontinuous grain boundary precipitation of lamellar γ' and b). incoherent δ precipitation emanating from the boundaries and travelling into the grains, enveloping γ'-depleted zones around them. Additionally, coarsening and dissolution of intragranular γ' is more pronounced in VDM 780 than in H282, when compared with the as-received microstructures.

In summary, both alloys display better mechanical performance at different conditions. VDM 780 is superior at lower temperatures (<850 ℃) with high operating stresses while H282 is more tolerant of higher operating temperatures at lower stresses. Overall, between temperature, time, and stress; temperature has the overpowering control. The

differences arising in γ' precipitate size scale, distribution, and V_f, evolution with temperature is revealed to have the most impact on the macroscopic response of these alloys. The current study provides an impactful comparison of these two alloys and paves way into designing new nickel superalloys for hot tooling applications.

References

1. Kracke, A. Superalloys, the most successful alloy system of modern times-Past, present, and future. In Superalloy 718 and Derivatives (2012) doi: 10.1002/9781118495223.ch2.

2. Roger C. Reed, The superalloys: Fundamentals and Applications. Cambridge: Cambridge University Press, 2002.

3. Lu, B.S. & Wang, L.G. & Huang, Y: Effect of deformation rate on interfacial heat transfer coefficient in the superalloy GH4169 hot forging process (2016). Applied Thermal Engineering. 108. 10.1016/j.applthermaleng.2016.07.167.

4. Kennedy, R.L.(2005). Allvac 718Plus, Superalloy for the Next Forty Years. Proceedings of the International Symposium on Superalloys and Various Derivatives. 1-14. 10.7449/2005/Superalloys_2005_1_14.

5. Xie, Xishan & Xu, Chunmei & Wang, Gailian & Dong, Jianxin & Cao, Wei-Di & Kennedy, Richard. (2005). TTT diagram of a newly developed Nickel-base superalloy - Allvac 718Plus. Proceedings of the International Symposium on Superalloys and Various Derivatives. 10.7449/2005/Superalloys_2005_193_202

6. Fedorova T, Rösler J, Klöwer J, Gehrmann B (2014) Development of a new 718-type Ni-Co superalloy family for high temperature applications at 750 °C. In: MATEC web of conferences, p 14 (2014).

7. Solís, C., Munke, J., Bergner, M. et al. Effect of heat treatment on microstructure and mechanical properties of VDM Alloy 780 Premium (2018) Metall and Mat Trans A 49: 4373. https://doi.org/10.1007/s11661-018-4761-6.

8. Casanova, A., Hardy, M. and Rae, C. (2014). Morphology and kinetics of grain boundary precipitation in alloy ATI 718Plus®. In 8th International Symposium

on Superalloy 718 and Derivatives doi:10.1002/9781119016854.ch45.

9. Solís, C., Munke, J., Bergner, M., Kriele, A., Mühlbauer, M., Cheptiakov, D., Gehrmann, B., Rösler, J. and Gilles, R. (2018). In situ characterization at elevated temperatures of a new Ni-based superalloy VDM-780 Premium. Metallurgical and Materials Transactions A, 49(9), pp.4373-4381.

10. C. Ghica, C. Solís, J. Munke, A. Stark, B. Gehrmann, M. Bergner, J. Rösler, R. Gilles, HRTEM analysis of the high-temperature phases of the newly developed high-temperature Ni-base superalloy VDM 780 Premium, Journal of Alloys and Compounds, Volume 814, 2020, 152157, ISSN 0925-8388, https://doi.org/10.1016/j.jallcom.2019.152157.

11. Pike, L. (2010). Long Term Thermal Exposure of HAYNES 282 Alloy. 645-660. 10.7449/2010/Superalloys_2010_645_660

12. "Origin: Data Analysis and Graphing Software". Originlab.Com, 2022, https://www.originlab.com/origin. Accessed 27 Aug 2022.

13. Polkowska, A., Polkowski, W., Warmuzek, M. et al. Microstructure and Hardness Evolution in Haynes 282 Nickel-Based Superalloy During Multi-Variant Aging Heat Treatment. J. of Materi Eng and Perform 28, 3844–3851 (2019). https://doi.org/10.1007/s11665-019-3886-0.

14. Joseph, C. (2015). Microstructural characterization of Haynes 282 after heat treatment and forging. CHALMERS UNIVERSITY OF TECHNOLOGY.

15. Hanning, Fabian, et al. "Investigation of the Effect of Short Exposure in the Temperature Range of 750-950 degrees C on the Ductility of Haynes (R) 282 (R) by Advanced Microstructural Characterization." *Metals* 9.12 (2019).

16. J.J. deBarbadillo,14 - INCONEL alloy 740H, Editor(s): Augusto Di Gian Francesco, Materials for Ultra-Supercritical and Advanced Ultra-Supercritical Power Plants, Woodhead Publishing, 2017, Pages 469-510, ISBN 9780081005521,

https://doi.org/10.1016/B978-0-08-100552-1.00014-2.

17. B.-A. Behrens, A. Bouguecha, I. LÃken, A. Klassen, D. Odening, Near-Net and Net Shape Forging, Comprehensive Materials Processing, Elsevier, 2014, Pages 427-446, ISBN 9780080965338, https://doi.org/10.1016/B978-0-08-096532-1.00323-X.

18. Louchet, F. (1995). A model of negative creep in nickel-based superalloys. *Scripta metallurgica et materialia*, *33*(6).

19. Williams, David B. and E. P. Butler. "Grain boundary discontinuous precipitation reactions." International Materials Reviews 26 (1981): 153-183.

20. E. I. Galindo-Nava, L. D. Connor and C. M. F. Rae, "On the Prediction of Yield Stress of Unimodal and Multimodal Gamma Prime Nickel-Base Superalloys," Acta Materialia, vol. 98, pp. 377-390, 2015.

21. Hawk, J. A., Cheng, T. L., Sears, J. S., Jablonski, P. D., & Wen, Y. H. (2015). Gamma prime stability in Haynes 282: theoretical and experimental considerations. Journal of Materials Engineering and Performance, 24(11), 4171-4181.

22. M. Donachie and S. Donachie, Superalloys: A technical guide. Materials Park: ASM International, 2002.

23. McDevitt, E. (2012). Effect of temperature and strain during forging on subsequent delta phase precipitation during solution annealing in ATI 718Plus Alloy. In Superalloy 718 and Derivatives doi:10.1002/9781118495223.ch23.

24. Sundararaman, M., Chen, W., Singh, V., & Wahi, R. P. (1990). TEM investigation of γ′ free bands in nimonic PE16 under LCF loading at room temperature. *Acta metallurgica et materialia*, *38*(10), 1813-1822.

25. Lavtar, L., Muhič, T., Kugler, G., & Terčelj, M. (2011). Analysis of the main types of damage on a pair of industrial dies for hot forging car steering mechanisms. Engineering Failure Analysis, 18(4), 1143-1152. doi: 10.1016/j.engfailanal.2010.11.002.